Journal of Geophysical Research: Space Physics

RESEARCH ARTICLE
10.1029/2018JA025442

Statistical Study of the Energetic Proton Environment at Titan's Orbit From the Cassini Spacecraft

L. H. Regoli[1,2,3,4], E. Roussos[1], K. Dialynas[5], J. G. Luhmann[6], N. Sergis[5], X. Jia[2], D. Román[2], A. Azari[2], N. Krupp[1], G. H. Jones[3,4], A. J. Coates[3,4], and I. J. Rae[3]

[1]Max Planck Institute for Solar System Research, Göttingen, Germany, [2]Climate and Space Sciences and Engineering, University of Michigan, Ann Arbor, MI, USA, [3]Mullard Space Science Laboratory, University College London, Holmbury St. Mary, UK, [4]Centre for Planetary Science at UCL/Birkbeck, London, UK, [5]Office for Space Research and Technology, Academy of Athens, Athens, Greece, [6]Space Sciences Laboratory, University of California, Berkeley, CA, USA

Abstract A statistical study of the energetic proton environment at Titan's orbit as captured by the MIMI/LEMMS and MIMI/CHEMS instruments is performed. The data analyzed cover all the dedicated flybys of Titan by Cassini as well as the orbit crossings that happen far from the moon. The energetic environment is found to be highly variable on timescales comparable to that of the duration of a flyby. Analysis of H^+ ion fluxes reveals a weak asymmetry in Saturn local time with the highest fluxes occurring in the premidnight sector of the magnetosphere. A correlation between the energetic ion fluxes and the location of Cassini in the magnetosphere with respect to the center of the current sheet can be observed. Finally, an empirical model of proton spectra for energies above 20 keV is derived based on fits to Kappa distribution functions. This model can be used to better understand the interaction of Titan with the magnetosphere and the energy deposition by energetic particles below the main ionospheric peak.

Key Points:
- Energetic particle environment at Titan's orbit is highly variable
- Ion data present SLT asymmetry with higher fluxes in the premidnight sector
- Derivation of empirical model of ion spectra based on Kappa distribution function is presented

Correspondence to:
L. H. Regoli,
lregoli@umich.edu

Citation:
Regoli, L. H., Roussos, E., Dialynas, K., Luhmann, J. G., Sergis, N., Jia, X., et al. (2018). Statistical study of the energetic proton environment at Titan's orbit from the Cassini spacecraft. *Journal of Geophysical Research: Space Physics*, *123*, 4820–4834. https://doi.org/10.1029/2018JA025442

Received 6 MAR 2018
Accepted 25 MAY 2018
Accepted article online 31 MAY 2018
Published online 16 JUN 2018

1. Introduction

The interaction of Titan with its surrounding environment is arguably one of the most complex interactions of its kind in the solar system. The mean orbital distance of the moon to Saturn is 20.3 Saturn radii (R_S), which locates it close to the magnetopause stand-off distance, described using a bimodal model with mean distances of 22 and 27 R_S by Achilleos et al. (2008), when crossing the subsolar point. As a consequence, while Titan spends most of the time in the outer region of the Saturnian magnetosphere, under strong solar wind conditions it can be located within the magnetosheath (Bertucci et al., 2008; Edberg et al., 2013) or in the unshocked solar wind (Bertucci et al., 2015).

Titan's orbit lies almost at the equator but due to the fact that Saturn's current sheet can move up and down into a bowl shape due to solar wind activity (Arridge et al., 2008), the moon can be located inside or outside the plasma sheet at any given time. This flapping motion of the current sheet, affected by magnetospheric dynamics, can be faster than the transit time of Cassini during dedicated flybys. This, together with the different trajectory geometries for different flybys, makes it possible for the plasma and field instruments to detect different plasma environments during the inbound and outbound parts of the trajectory (Simon et al., 2013).

Since Titan does not possess an internal magnetic field (Backes et al., 2005; Wei et al., 2010), its atmosphere and ionosphere interact directly with the different environments just described, creating a unique moon-magnetosphere interaction when located inside the magnetosphere. When located upstream of the Saturnian bow shock, the interaction is very similar to that of Mars (e.g., Brain et al., 2010; Brecht & Ledvina, 2006) or Venus (e.g., Russell et al., 2006; Slavin et al., 1980) with the solar wind (Bertucci et al., 2015). When located in the magnetosheath, Titan has been observed to retain signatures of the Saturnian magnetic field in the conducting ionosphere, something that has been referred to in the literature as fossil fields (Bertucci et al., 2008).

During the Cassini era, it became clear that the north-south orientation of the magnetic field observed during the Voyager 1 flyby (Neubauer et al., 1984) was not common, with only a single flyby reported in the literature, namely, T70 (Simon et al., 2013), having occurred during such conditions. For this reason, different efforts to

classify the different environments at which Titan can be located have been undertaken using different data sets provided by different instruments on board Cassini.

Using electron data from the Electron Spectrometer (ELS), part of the Cassini Plasma Spectrometer (CAPS), and from the Low Energy Magnetospheric Measurement System (LEMMS), part of the Magnetospheric Imaging Instrument (MIMI), Rymer et al. (2009) identified four different regions according to the characteristic thermal electron environment. These regions are plasma sheet (high energy and density), lobe-like (high energy, low density), magnetosheath (low energy and high density), and bimodal (two superimposed populations). This classification was extended by Smith and Rymer (2014) to include all the data gathered at Titan's orbit (with and without Titan present) by the CAPS/ELS instrument until it was switched off in 2012 after 83 flybys.

A similar classification was made using ion data for the first 54 flybys from the CAPS/IMS instrument by Németh et al. (2011). They also looked at ion composition, finding short events with enhanced heavy ion densities occurring when Cassini crossed the narrow central sheet (Németh et al., 2011).

Being located in the outer magnetosphere, the planetary magnetic field configuration at Titan's orbit differs significantly from that of a dipolar configuration. Due to the fast rotation of the planet and the presence of heavy ions, the centrifugal force causes the partially corotating plasma to be confined near the equatorial regions, creating a current sheet that is present at all local times, although with varying thickness (Krimigis et al., 2007). All of this means that the magnetic field can also be used to estimate the location of Titan with respect to the magnetic equator. Using data from the Magnetometer (MAG) instrument, Simon et al. (2010) classified the magnetic environment during the TA to T62 flybys. The classification was later extended to include the data until the T85 flyby (Simon et al., 2013).

More recently, Kabanovic et al. (2017) provided an empirical model of the magnetic environment at the moon's orbit using magnetic field data obtained by Cassini. They found a perturbed field configuration close to noon local time, regardless of the season, while a dependence on the season is present in the nightside due to the change in the orientation of bowl-shaped current sheet.

The energetic plasma environment, specifically protons with energies from 27 to 255 keV, was studied by Garnier et al. (2010) for all the flybys and orbit crossings from Saturn Orbit Insertion (SOI) until January 2008, almost at the end of Cassini's Prime Mission. The then total number of crossings accounted for 39 dedicated flybys and 33 crossings far from Titan. In their work, they analyzed data from the MIMI suite, concentrating on the LEMMS and the Ion Neutral Camera (INCA) instruments. For the former, they looked at the energetic proton data (with energies between 27 and 255 keV) far from the region where the disturbances introduced by Titan are appreciable. By looking at mean fluxes for the channels analyzed and studying their correlation with Saturn local time (SLT), they found larger fluxes in the postmidnight to dawnside.

It is evident from the descriptions provided above that classification of Titan's upstream environment is the least developed in terms of energetic charged particles. The study of Garnier et al. (2010) provides some insights but covers only a small time period and is limited in energy coverage. It provides no detailed information about the shape and intensity of energetic ion spectra. With the other classifications in mind (by the CAPS and MAG instruments) and with the Cassini mission completed, we have the opportunity to update and extend the results of Garnier et al. (2010) providing a more detailed description of Titan's energetic particle environment. The availability of an empirical model of energetic particles is necessary to complement the study of how Titan interacts with the magnetospheric environment and how the energy deposition into the atmosphere changes with upstream conditions.

Cassini performed the first dedicated flyby of Titan on 26 October 2004. During this flyby, known as the TA flyby, Cassini traveled, with an altitude at closest approach (CA) of 1,174 km, below the main ionospheric peak, located at around 1,200 km. Cravens et al. (2005) compared the results obtained by the Radio and Plasma Wave Science instrument during this flyby with those obtained using a photochemical model along the track of the spacecraft. They showed that by just considering photoionization (without the inclusion of electron impact ionization), the production rate predicted by the model was significantly lower than what the data showed, making it necessary to consider the magnetospheric input as well.

Edberg et al. (2015) looked at the electron densities in Titan's ionosphere at different local times. After filtering out the ionization by solar extreme ultraviolet using a photochemical model, they found higher densities during flybys that occurred around the midnight sector of the magnetosphere and lower densities around noon. They suggested that this difference could be due to ionization from magnetospheric sources.

Using data obtained by the MIMI/LEMMS instrument during the T5 flyby, Cravens et al. (2008) calculated production rates from precipitating H^+ and O^+ from the magnetosphere of Saturn. They found that the these ions can contribute to the ionization of the atmosphere at altitudes between 500 km and 1,000 km, below the main ionospheric peak, which is mainly produced by solar extreme ultraviolet radiation, a result confirmed through test particle simulations by Regoli et al. (2016).

Gronoff et al. (2009) also analyzed the role of energetic electrons in the ionization of Titan's atmosphere during the T5 flyby and concluded that the geometry of the draped field lines has a significant influence on the local electron fluxes. Similar results were obtained by Smith et al. (2009) by looking at energetic neutral atom (ENA) emissions produced by precipitating protons and detected by the MIMI/INCA instrument.

In terms of neutral particles, Brandt et al. (2012) studied the exosphere of Titan using ENA measurements from the INCA instrument. They found an H_2 exosphere that extends to about 50,000 km and also estimated the precipitation of ENAs to be comparable to that of energetic ions. This led to the suggestion that for any study analyzing the energy budget at Titan's atmosphere, ENAs need to be accounted for.

In this work we analyze the energetic environment at Titan's orbit, with a focus on energetic protons. Using data from the LEMMS and Charge Energy Spectrogram (CHEMS) instrument, we develop a method to characterize the proton fluxes and distribution encountered at Titan's orbit at different locations in the magnetosphere, as well as an empirical model of the energetic proton environment. The results of the present work are particularly interesting for the ionization of Titan's atmosphere and for understanding ENA emissions from Titan's exosphere, as observed by Cassini's INCA detector.

2. Instrumentation and Data Set

Cassini had a series of instruments devoted to the study of charged particles at different energy levels. Among those, CAPS and MIMI were designed to perform in situ measurements of the fluxes of charged particles with different energies in Saturn's magnetosphere.

CAPS (Young et al., 2004) was composed of three instruments, namely, ELS, the Ion Mass Spectrometer (IMS), and the Ion Beam Spectrometer. Among the three of them, ELS and IMS are of special interest when it comes to characterizing the low-energy environment of the Saturnian magnetosphere. ELS was used to characterize the plasma environment at which Titan was encountered at each of the flybys for which CAPS data are available (Rymer et al., 2009). Due to an electrical failure of the spacecraft, CAPS was switched off shortly after the T83 flyby that took place in May 2012.

CAPS covered the low-energy part of the spectrum, with ELS reaching energies of up to 28 keV and IMS reaching energies of up to 50 keV. This was neatly complemented by MIMI (Krimigis et al., 2004), composed by LEMMS, CHEMS, and INCA.

The data used in the present study were collected by the LEMMS and CHEMS instruments. LEMMS was mounted on a rotating platform intended to provide 360° coverage on the spacecraft's *x*-*z* plane. The platform, however, stopped working at the beginning of 2005, leaving the instrument looking into a fixed direction (Krupp et al., 2012). This limited the pitch angle coverage of the instrument, although at Titan's orbit, as reported by Garnier et al. (2010), the ion distribution is quasi-isotropic.

LEMMS consisted of a double-ended telescope. The two ends of the instrument measured different energy ranges, one being labeled as *low energy* and one as *high energy*. The low-energy end was able to measure ions with energies between 27 keV and 4 MeV and electrons from 18 to 832 keV, while the high-energy end could measure ions with energies from 1.4 to 160 MeV/N and electrons from 0.1 to several tens of MeV (Krupp et al., 2009).

For this study, only ion data gathered by the low-energy telescope are used. The corresponding channels on the LEMMS instrument are labeled A0 to A7 and the energy range for each one of these channels is presented in Table 1. For most of the time when Cassini was in the outer magnetosphere near Titan's orbit, the highest-energy channels of the instrument do not measure any fluxes above the detection threshold. For this reason, some of the analyses presented here will focus on the lowest-energy channels.

CHEMS was a mass spectrometer capable of distinguishing between ion species and their charge state, most importantly H^+ and W^+ ions, the two major magnetospheric species present at Titan's orbit (e.g., Arridge et al., 2011; Dialynas et al., 2009; Sergis et al., 2007; Thomsen et al., 2010). The instrument was composed of

Table 1
Energy Ranges Covered by Individual Channels of the MIMI/LEMMS Instrument, Adapted From Krupp et al. (2009)

Ion channel	Energy range (keV)
A0	27–35
A1	35–56
A2	56–106
A3	106–255
A4	255–506
A5	506–805
A6	805–1,600
A7	1,615–4,000

three telescopes, each one containing an electrostatic analyzer to filter particles based on their energy/charge followed by a time-of-flight analysis to determine the mass of the detected ion. The central telescope was fairly well aligned with the low-energy telescope of LEMMS. In terms of energies, CHEMS covered the range between 2.8 keV and 220 keV.

For all the analyses presented in the following sections of the paper, data collected between SOI and the beginning of 2017 are used. Since the focus of the paper is on the energetic H^+ environment at Titan's orbit, the data are filtered to cover the L shell range between 19 and 21 R_S and the latitude is also limited by only including data collected within 1 R_S of the equatorial plane. In general, higher latitudes can be considered (from where fluxes can be mapped to Titan's orbital plane); but due to the ambiguity of magnetic field models for Saturn's magnetosphere at Titan's distance, we restrict our study near the equatorial plane. For some of the analyses, subsets of the described data set are used, as indicated at the beginning of the corresponding section.

When analyzing data collected during dedicated flybys, the interaction region (defined as the region of the magnetosphere affected by the presence of the moon) is removed from the data to ensure that only the magnetospheric environment is taken into account.

In terms of accumulation time, two different sets were used for the study. When analyzing fluxes (sections 3 to 5), 10-min averaged data were used, while for the Kappa distribution analysis (section 6) 30-min averaged data were used. These accumulation times provide enough smoothing of the data while still capturing the possible spatial variations.

Taking into account the spatial constraints just mentioned, it took about 4 hr for Cassini to fly through the region of interest. This translates into approximately 24 data points available for each of the flybys and orbit crossings for the analysis for fluxes and about eight spectra for the Kappa distribution fits.

3. Dependence of the Energetic Ion Fluxes on the Local Plasma Environment

In order to correctly interpret any results involving the fluxes of energetic ions, it is important to determine whether these fluxes are affected in any way by the location in the magnetosphere at which Cassini was at the time the data were obtained (as is the case for lo-energy ions and electrons). For this, the classification introduced by Rymer et al. (2009) is used, where six different categories were defined, namely, plasma sheet (hereafter referred to as category 1), lobe-like (2), magnetosheath (3), bimodal (4), mixed (5), and unclassified (6). On 1 December 2013, Titan was encountered by Cassini while in the unshocked solar wind (Bertucci et al., 2015) so an extra category, namely, solar wind (7), will be included as well.

The first three categories are, as their names imply, related to the specific locations inside Saturn's magnetosphere. Bimodal spectra contain two different electron populations which were linked by Rymer et al. (2009) to an enhanced pickup ion environment. Mixed means that Cassini crossed more than one environment during the flyby or pass. Finally, unclassified means that the observed spectrum does not fit in any of the first four categories, but at the same time it is not uniform enough as to justify the creation of a new category.

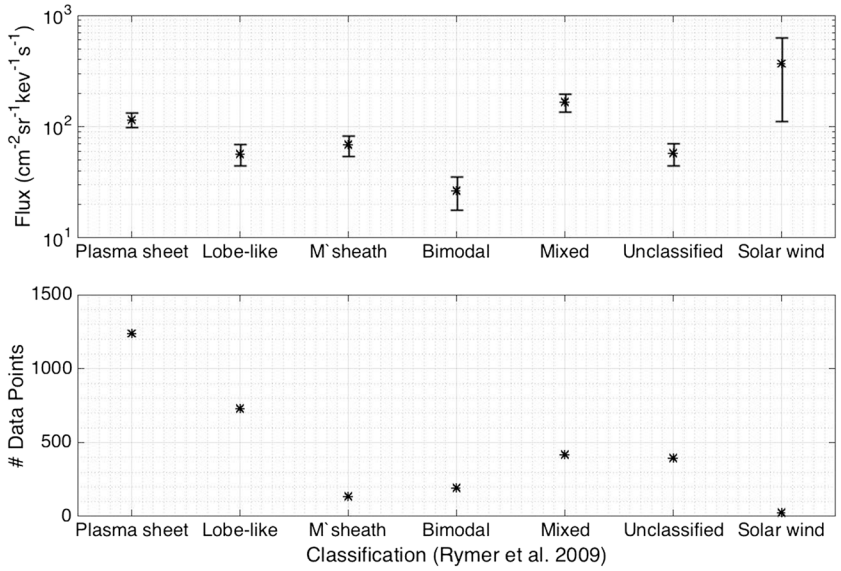

Figure 1. Median of ion fluxes from the A0 channel (27–35 keV) collected during the first 83 flybys plus T85 and T96, organized by plasma environment (top panel) with the error bars representing the median of the standard deviation of the measurements. Number of data points for each environment (bottom panel).

Here we look at the ion channel with the lowest energies from LEMMS (namely, A0, with energies from 27 to 35 keV) in order to determine whether a correlation exists between the observed average fluxes and the category in which each of the flybys occurred. We only use the lowest-energy channel since we are interested here in global trends in the magnetosphere. An analysis containing the full distribution of high-energy particles is presented in section 6.

The top panel of Figure 1 shows a plot of the median fluxes of the data from the A0 channel obtained during each of the first 83 flybys plus T85 and T96, and a subset of the orbit crossings for which the environment classification has been published (Smith & Rymer, 2014). Apart from all the flybys and orbit crossings with classification from the CAPS instrument, T85 is included because it was another magnetosheath flyby (Edberg et al., 2013) and T96 because it was the only solar wind flyby recorded by Cassini (Bertucci et al., 2015). The bottom panel shows the number of data points available at each environment.

Table 2 shows the median values plotted in Figure 1 together with the number of data points available for each case. The data points correspond to all the spectra collected for the analysis and not to individual events.

Without taking into account the mixed and unclassified data points, from the median fluxes presented in Figure 1 and Table 2, it can be seen that the A0 channel fluxes are indeed influenced by the moon's location, with the solar wind fluxes being the most strongly influenced followed by the plasma sheet ones. Since there is only one flyby occurring in the solar wind, the statistical significance of this result cannot be asserted, although

Table 2
Median of Fluxes Detected by the LEMMS A0 Channel (in $cm^{-2} \cdot sr^{-1} \cdot kev^{-1} \cdot s^{-1}$) and Number of Available Data Points

Classification	A0 flux (median)	Number of data points
Plasma sheet	115.97	1,236
Lobe-like	56.96	731
Magnetosheath	68.69	135
Bimodal	26.80	192
Mixed	167.01	418
Unclassified	57.58	393
Solar wind	371.16	24

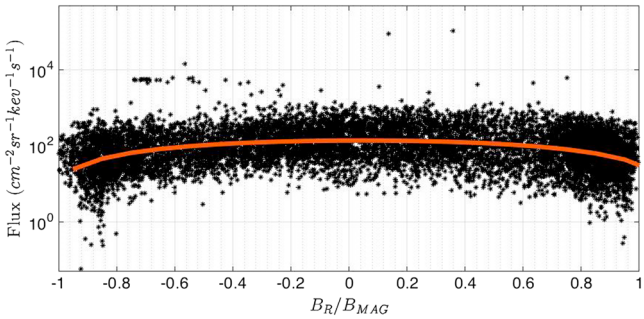

Figure 2. Ion fluxes from the A0 channel of the MIMI/LEMMS instrument versus location with respect to the center of the current sheet. The orange line shows a second-order polynomial fit to the median of the data.

the fact that the magnetopause and the bow shock boundaries were pushed beyond the orbit of Titan directly implies large solar wind fluxes.

In contrast to what is observed in the thermal plasma data from the CAPS instrument, the fluxes in the magnetosheath are lower than those encountered in the plasma sheet. At the same time, they are slightly higher than those in the lobes, although an important overlap between both classifications exists. From the number of available data points, it is also evident that the quality of the statistics from different environments is different, with the plasma sheet and the lobe regions inside the magnetosphere being the better sampled.

Another way of looking at the data while considering all the data points available is to make a rough distinction between plasma sheet and lobes based on the magnetic field data. This can be achieved by plotting the fluxes versus the ratio between the radial component of the magnetic field and the magnitude of the field. When this ratio is close to zero, it means the magnetic field is almost perpendicular to the orbit plane, meaning that the data were collected close to the center of the current sheet. Figure 2 shows a scatter of all the A0 channel measurements included in the study plotted against $B_r/|B|$, together with a second-degree polynomial fit that shows the trend toward higher fluxes closer to the center of the current sheet and lower fluxes at the lobes.

In general, although with some overlap between the lobe-like and magnetosheath regions, the data follow a trend that is expected, with the fluxes in the plasma sheet being higher than those in the lobes. Using a single channel, though, provides an incomplete description of the environment.

In addition to the difference in kinetic energy, the overall shape of the distribution is another factor that makes it possible to use the thermal plasma data for classification but not the energetic data. The Rymer et al. (2009) and Németh et al. (2011) classifications rely on two main factors to define the different categories, namely, flux and energy of the peak of the distribution. While the fluxes can vary for energetic data as well, the peak of the distribution is always located at the lowest-energy channels of the MIMI instrument.

4. Ion Fluxes Over Time

Figure 3 shows the ion fluxes detected by the A0 channel of the instrument between Saturn orbit insertion (SOI) in 2004 and the beginning of 2017. The plot includes all the data gathered during that period at Titan's orbit, regardless of the plasma environment or local time. It also includes both flybys and orbit crossings.

It can be seen that no clear seasonal dependence is present, and overall, the fluxes are highly variable. As representative of higher or lower fluxes than the general trend, five specific periods are highlighted in the plot. These correspond to the times listed in Table 3 together with some relevant parameters.

The three highlighted time periods with high fluxes coincide with two dedicated flybys, namely T32, T78 and T96. T32 was the first flyby of the mission that occurred with Titan inside the magnetosheath. The fact that Titan was located outside the magnetosphere means that the solar wind was energized and, even after being slowed down past the bow shock, the distribution of ions detected by Cassini was energized enough that the LEMMS instrument was able to capture an enhanced flux of particles.

The case of T78 is quite different. While T32 occurred at the noon sector of the magnetosphere, specifically at 13.56 SLT, T78 occurred in the afternoon sector, at 17.55 SLT. Furthermore, the flyby was classified using MAG data by Simon et al. (2013) as having taken place under plasma sheet conditions. At the time of the flyby,

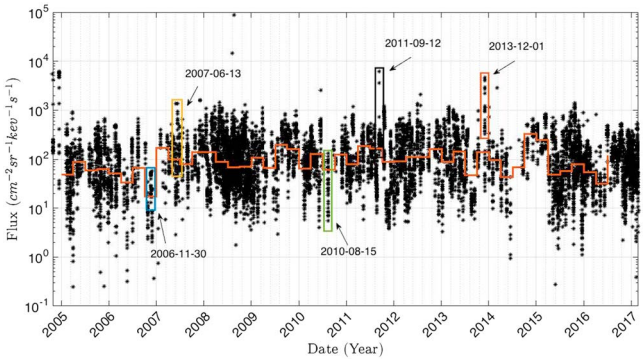

Figure 3. Ion fluxes from the A0 channel of the MIMI/LEMMS instrument sampled between 2004 (SOI) and beginning of 2017. The orange line shows the median of the fluxes for consecutive periods of time covering 3 months.

CAPS was switched off, so no classification from the low-energy plasma point of view is available (Smith & Rymer, 2014).

The third highlighted point corresponds to the T96 flyby, that took place at a time when the magnetosphere was compressed by the arrival of an ICME, and it corresponds to the only flyby during the Cassini mission when Titan was observed in the solar wind.

High fluxes are also visible for the very first data set which corresponds to the TA flyby. Being the first flyby of the mission, TA was studied in detail using different data sets and simulations and it was found that the fluxes were relatively high, comparable to those observed by Voyager 1 (e.g., Backes et al., 2005; Cravens et al., 2005; Hartle et al., 2006).

For the case of low fluxes, two times are highlighted in Figure 3. Both of them correspond to crossings of Titan's orbit, with the first data point having been collected at 2.16 SLT and the second one at 15.9 SLT. The selection of these data points was solely based on their relatively low fluxes as shown in Figure 3 and, at first glance, no noticeable features that could explain the low fluxes are present.

Given their lack of interaction with the solar wind boundaries, solar energetic particles (SEP) can penetrate the magnetosphere and thus serve as a proxy for the solar wind activity when Cassini was inside the magnetosphere of Saturn. A series of these events was identified by Roussos et al. (2017). The data points for the A0 and A5 channels that fall within the period of time when these SEP events were detected are highlighted in orange in Figure 4.

In general, although SEP events increase the fluxes in the highest-energy channels of the LEMMS instrument (Roussos et al., 2017), the effect does not seem to be as strong in the lowest-energy channels. This is not completely unexpected, given that the ability of a particle to penetrate the bow shock depends on the particle's energy, and those detected by the A0 channel might simply not have the energy needed to do so. This is apparent when comparing the fluxes of the SEP events in both channels shown in Figure 4. While those from the A0 channel show no special trend, the ones detected by the A5 channel do have a bias toward higher fluxes.

Table 3
Characteristics of Four Selected Data Points for Ion Fluxes From the A0 Channel (Fluxes in $cm^{-2} \cdot sr^{-1} \cdot kev^{-1} \cdot s^{-1}$)

Date	A0 flux	SLT	Flyby/Pass	Classification
2006-11-30	57.15	2.17	Pass	Lobe-like
2007-6-13	1.36×10^3	13.56	Flyby (T32)	Magnetosheath
2010-8-15	130.02	15.90	Pass	Current sheet
2011-9-12	6.15×10^3	17.69	Flyby (T78)	Current sheet
2013-12-1	4.62×10^3	12.37	Flyby (T96)	Solar wind

Note. Dates are formatted as year-month-day.

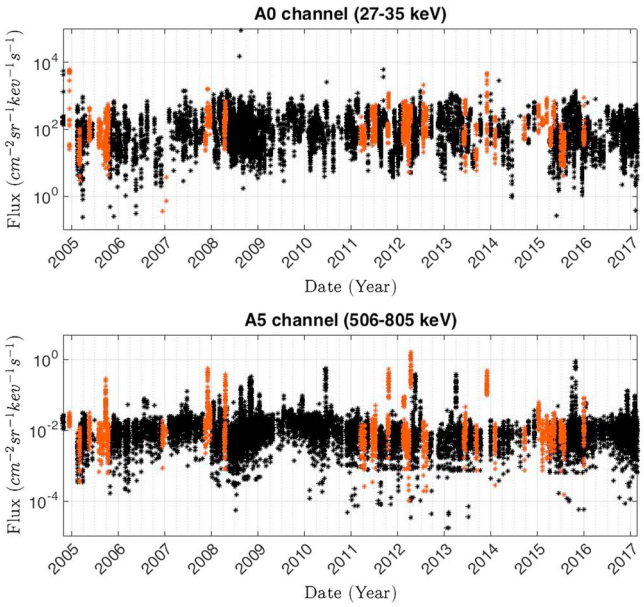

Figure 4. Ion fluxes from the A0 (top) and A5 (bottom) channels of MIMI/LEMMS showing periods when solar energetic particle events were observed at Saturn highlighted in orange.

5. Average Fluxes

In this section, the local time dependence of the energetic ion fluxes is analyzed. For this, all the data available from the lowest-energy ion channel (A0) between SOI and the beginning of 2017 are taken into account.

Figure 5 shows a plot of the median ion fluxes versus SLT divided into 2-hr bins for the two main magnetospheric environments, namely, current sheet (top) and lobe-like (bottom). Since the data are being divided by magnetospheric environment, only those times listed in Rymer et al. (2009) and Smith and Rymer (2014) are used. Both plots show the number of data points available at each SLT bin. The sampling is rather low for most bins, and for some of them there are no points available at all. The dayside/nightside asymmetry reported by Garnier et al. (2010) is not observable, although their analysis did not discern between magnetospheric environments.

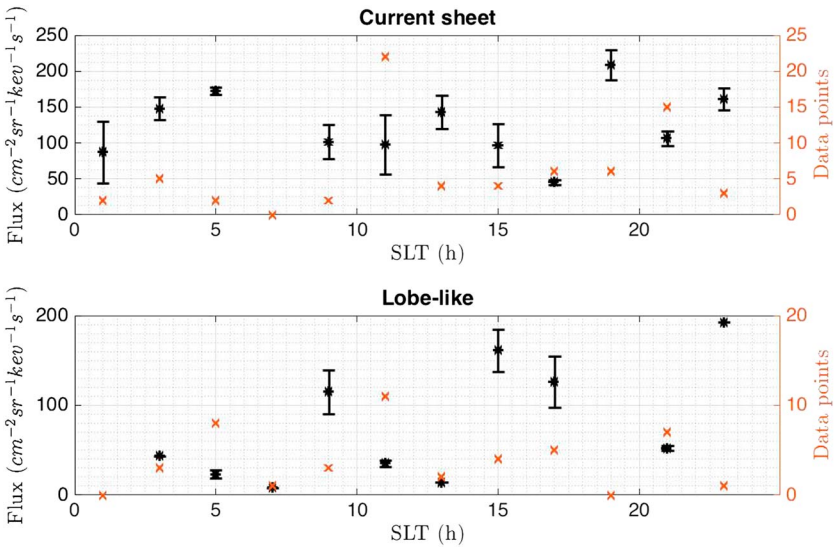

Figure 5. Median of ion fluxes from the A0 channel at two different magnetospheric environments, namely, current sheet (top panel) and lobe-like (bottom panel). The error bars correspond to the standard error of the medians. The right axes of the plots show the number of data points available at each Saturn local time bin.

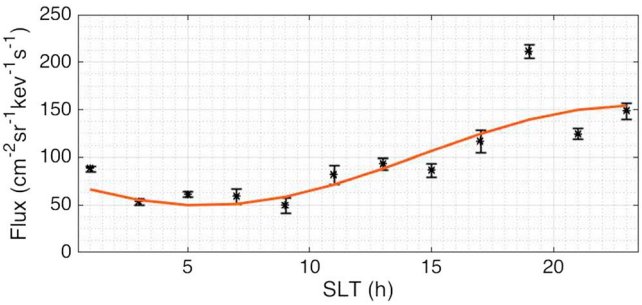

Figure 6. Median of ion fluxes from the A0 channel. The error bars correspond to the standard error of the medians and the orange curve shows a sinusoidal fit to the data.

When the environment restriction is removed, the plot shown in Figure 6 is obtained. In this plot an SLT asymmetry seems to be present, with the largest fluxes present between the afternoon and premidnight sector of the magnetosphere. However, the sampling bias observed in Figure 5 shows that many of the measurements taken in the nightside (especially in the premidnight sector, where fluxes seem to be higher) were made when Titan was in the current sheet, a region that, as shown in Figure 1, presents larger fluxes of energetic particles.

Part of the asymmetry in SLT observed in the electron densities in the ionosphere, as reported by Edberg et al. (2015) can be due to this sampling bias. While energetic particles are expected to penetrate below the altitude of Cassini's CA (Cravens et al., 2008; Regoli et al., 2016), part of the incident population could have grazing angles large enough that they will indeed deposit their energy at higher altitudes.

6. Analysis of Energetic H^+ Spectra using Kappa Distributions

Kappa distributions were first introduced by Vasyliunas (1968) to describe the spectra of plasma populations that could not be described with Maxwellian distributions in the Earth's magnetosphere and have since then been used to describe populations in other planetary magnetospheres (Dialynas et al., 2017) and plasma environments (e.g., Livadiotis, 2015; Livadiotis & McComas, 2013). In this study we use a simplified version of the original distribution that was described in Dialynas et al. (2009), based on a function introduced by Mauk et al. (2004) for the study of energetic ions in the Jovian magnetosphere.

Due to the energy distribution of particles in the magnetosphere, the MIMI/LEMMS and MIMI/CHEMS instruments capture the high-energy tail of a Kappa distribution centered at low energies that is detected by the CAPS instrument (Dialynas et al., 2009; Young et al., 2005). The high-energy fluxes have been organized by the value of the parameters of a Kappa distribution for the equatorial magnetosphere of Saturn, but no specific analysis for Titan's orbit has been made thus far, apart from the fact that the Dialynas et al. (2009) study included data collected by Cassini only until July 2007. In this section, a modified Kappa distribution function [equation (1)] is used with the aim of providing an empirical model of the fluxes of energetic particles at Titan's orbit.

$$j = C \cdot E[E + kT(1 + \kappa)]^{-(1+\kappa)} \tag{1}$$

Figure 7 shows two examples of the combined LEMMS and CHEMS spectra used in this study for two different times, together with the corresponding result of the fitting process. As visible from both spectra shown, the Kappa distribution function provides a good description of the plasma population with energies above 20 keV, whereas below that threshold, the distribution seems to be closer to an inverse power law, which is most likely representative of a second Kappa distribution that peaks at lower energies (Dialynas et al., 2009). For instance, Young et al. (2005) showed broad peaks of ions at local corotation speeds. This change in the distribution is particularly visible in the right-hand panel of Figure 7 and it implies that the results presented in this section in terms of an empirical model of the fluxes are only valid for energies above 20 keV.

Due to the already described variabilities of the outer magnetosphere, when analyzing the results of the fitting process the different possible sources of this variability need to be considered. These include location where the data were collected with respect to Saturn (SLT), location with respect to the current sheet (magnetic latitude), and whether the data were collected inside or outside the magnetosphere (only relevant for flybys or passes that occurred close to the subsolar point, or close to 12 SLT).

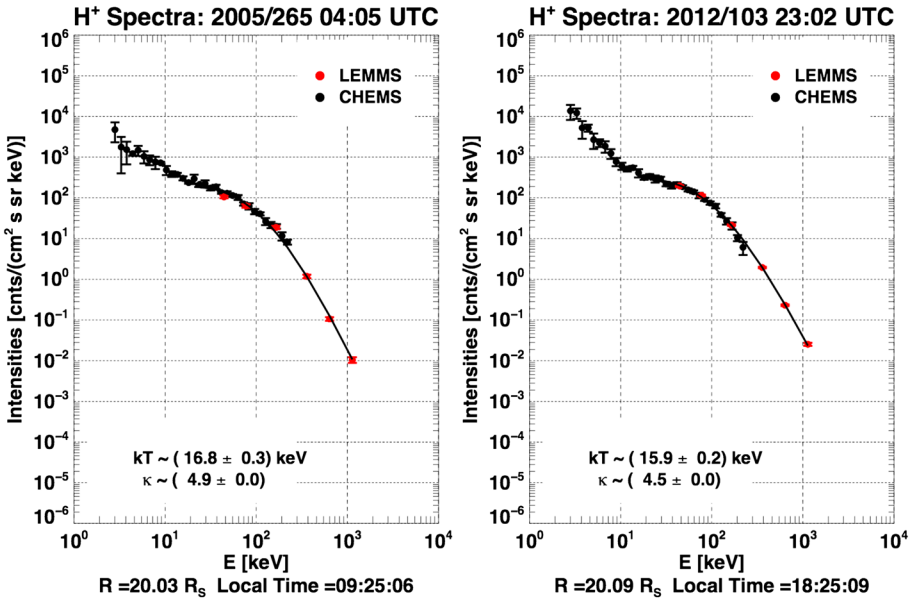

Figure 7. Combined LEMMS and CHEMS spectra and result of the fitting process for two different time periods. The error bars correspond to the standard deviation of the measurements.

Figure 8 shows the results of organizing the κ, kT, and C parameters with respect to SLT. In the cases of κ and kT it can be seen that the values are in good agreement with what was reported by Dialynas et al. (2009) for the outer magnetosphere. However, no clear trend is present in any of them.

Since most plasma sources in Saturn's magnetosphere are located in the inner region (with the main source, Enceladus, at a radial distance of 4 R_S), by the time the plasma is transported outward, any SLT asymmetries that could be originally present are smoothed out. This was shown by Dialynas et al. (2013) where they analyzed ion distributions from the MIMI instrument at radial distances between 5 and 20 R_S and showed that the inner magnetosphere presents significant structure (especially on the dayside) that decreases with increasing L-shell.

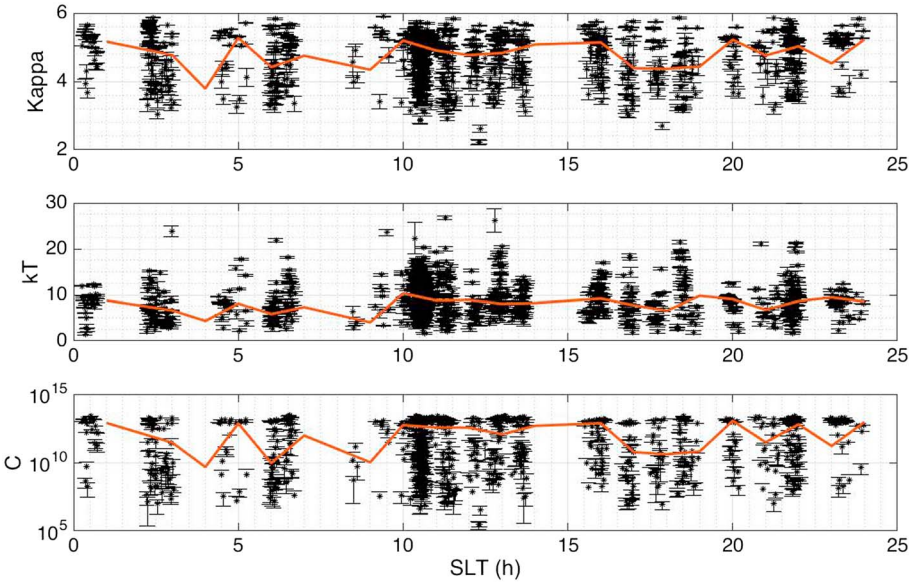

Figure 8. Parameters κ (top panel), kT (middle panel), and C (bottom panel) organized by Saturn local time. The data points correspond to the median of all the values at each Saturn local time bin and the error bars represent the standard deviation.

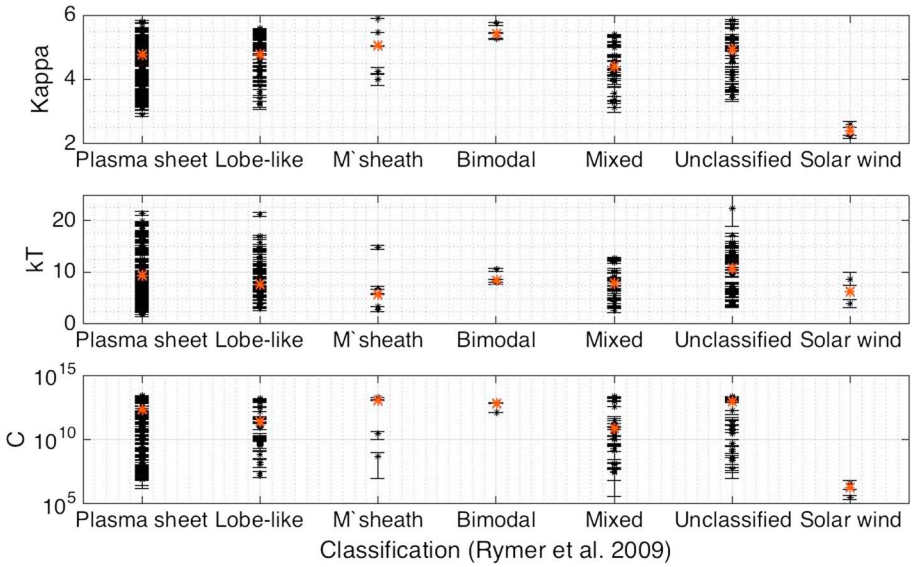

Figure 9. Parameters κ (top panel), kT (middle panel), and C (bottom panel) organized by magnetospheric environment according to Rymer et al. (2009) classification. The orange points correspond to the median of all the values at each SLT bin and the error bars represent the standard deviation.

Figure 9 shows the same parameters from the fits, this time organized by plasma environment using, once again, the classification from Rymer et al. (2009).

For the four well-defined environments all the three parameters show a similar trend, with the lowest values present for solar wind conditions, followed by plasma sheet, lobe-like, and magnetosheath conditions, where the maximum values are observed. There is, however, a significant spread in the data, another reflection of the variability of the energetic environment.

Table 4 presents the obtained median values of the three parameters. The κ parameter indicates the shape of the distribution, with a larger value meaning a more thermalized population. For this reason, it is interesting to analyze the κ value obtained for each environment.

The classification used was obtained using thermal electron data, and thus the link to energetic ions might be weak. This makes it difficult to interpret the results obtained, especially for cases like the bimodal distribution, which is based on an extra source of thermal electrons that might not be linked at all to energetic particles. For similar reasons, the results for the mixed and unclassified environments are only useful in a statistical sense and a physical interpretation is difficult to be derived.

For the other four environments, while the link between the thermal electron data and the energetic particles might be, at best, weak, some physical interpretation can be given to the results, keeping in mind that the statistical uncertainty of the values obtained is significant when compared to the difference between the

Table 4
Median Values of the Three Parameters of the Kappa Distribution Function Organized by Magnetospheric Environment

Classification	Kappa	kT	C	STD(C)
Plasma sheet	4.78	9.31	2.15×10^{12}	7.68×10^{12}
Lobe-like	4.78	7.64	2.47×10^{11}	4.99×10^{12}
Magnetosheath	5.04	5.75	1.13×10^{13}	8.12×10^{12}
Bimodal	5.43	8.37	5.74×10^{12}	3.08×10^{12}
Mixed	4.41	7.90	7.39×10^{10}	7.41×10^{12}
Unclassified	4.93	10.80	8.57×10^{12}	7.00×10^{12}
Solar wind	2.42	6.30	2.02×10^{6}	2.40×10^{6}

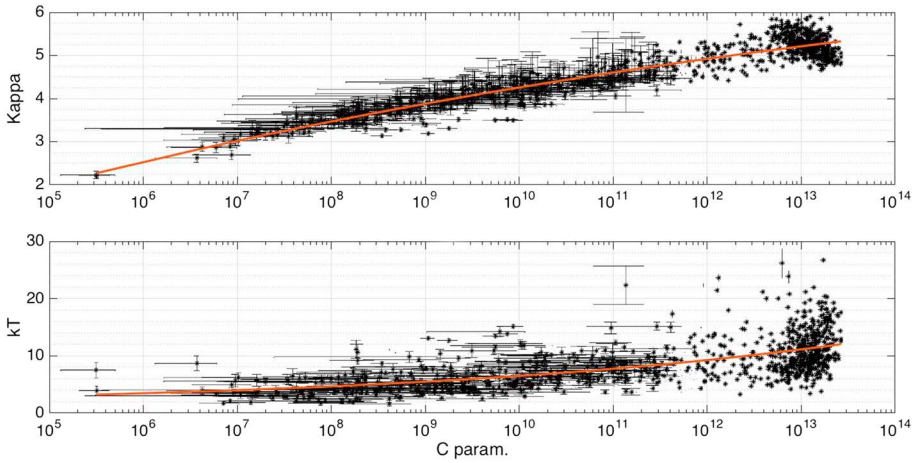

Figure 10. Correlation between different parameters of the Kappa distribution function [equation (1)]. The blue points are the values obtained from the fits while the colored curves represent different fits to the data.

values at specific environments. In general, the value of κ obtained for the solar wind is consistent with results reported in the literature (see, for instance, Table 1.1 in Livadiotis, , Livadiotis,).

The fact that, on average, the value of κ at the magnetosheath is larger than that at the plasma sheet and the lobes could be related to a thermalization of the solar wind plasma. However, the shape of the distribution will also depend on external parameters such as the Alfvén mach number and the plasma beta (e.g., Thomsen et al., 2018) at any given point and these values will necessarily be smoothed by the averaging performed in the analysis presented here.

In order to simplify the environment description, we have also looked for correlation between the three spectrum coefficients, so that we can reduce the free parameters of the spectrum from three to one. In terms of interdependence of the parameters, the plots from Figure 10 show the κ (top panel) and kT (bottom panel) parameters plotted against C.

The black points in both panels show the respective values obtained from the fits described above together with the error bars that are obtained from the quality of the fits. In addition, the two orange curves represent fits to the data.

Both plots show a power law dependence [equations (2) and (3), respectively], with a spread present for large values of C, where most of the points are concentrated (about half of the fits throw a value for C that is larger than 5×10^{12}). The goodness of the fit in terms of R^2 for the κ versus C case is 0.8757 and for the kT versus C case is 0.3672. This difference is already visible in Figure 10 from the larger spread of kT for low values of C.

$$\kappa = -9.915 \cdot C^{-0.03768} + 8.421 \tag{2}$$

$$kT = 0.7155 \cdot C^{0.08844} + 1.028 \tag{3}$$

The combination of the values of C provided for each magnetospheric environment together with the relations from equations (2) and 3 provide a description of the energetic particle fluxes at different environments.

7. Discussion and Conclusions

During the time orbiting Saturn, Cassini sampled different regions of the magnetosphere gathering enough data to understand part of the dynamics of the plasma circulation. Still, due to the size of the magnetosphere, the coverage is far from perfect. If we add this to the fact of only having a single spacecraft to analyze the dynamic processes that take place in the outer regions of the magnetosphere, characterizing the magnetospheric environment at Titan's orbit is a very challenging task.

Given that about 50% of the particle pressure in the magnetosphere of Saturn is contributed by the energetic particles (Sergis et al., 2009), understanding the fluxes from a statistical point of view is important to provide a

comprehensive model of the interaction of Titan with the Saturnian magnetosphere. In addition, an empirical model of the ion fluxes can help constrain the energy deposition by energetic particles that affect mainly the ionospheric densities below the main ionospheric peak.

While some progress has been made with the magnetic field and low-energy particle data, few studies have focused on the high-energy plasma. In this paper, we analyzed data from the MIMI/LEMMS and MIMI/CHEMS instruments in order to study, from a statistical point of view, the behavior of energetic H^+ ions. Toward this, we looked at the mean fluxes detected by LEMMS and also at the energy distribution by fitting Kappa distribution functions to the data.

Based on the analyses detailed on the paper, we conclude that the energetic environment is extremely variable. As expected based on prior studies and on this one, when looking at ions in the keV and MeV scale, we are only looking at the high-energy part of the total particle distribution and these particles, due to their high kinetic energy, are not as cleanly organized by their location with respect to the center of the plasma sheet as thermal particles are.

Fluxes in the higher-energy channels are notably increased during SEP events. This increase in the fluxes can be related to acceleration processes arising from the arrival of the SEPs or to the fact that solar wind ions with very high energies can penetrate the magnetosphere, thus reaching the moon even when located downstream of the magnetopause. In both cases, this implies that the energy deposition in the atmosphere might be affected during periods of enhanced solar activity, something that needs to be further analyzed to evaluate how the ionosphere below the main peak is affected.

With the aim of providing an empirical model of the energetic particle environment, instead of looking at the fluxes of a single energy channel, a better approach is to look at the distribution of particles. At the energies analyzed in this study, we see the high-energy tail of a Kappa distribution that peaks at low energies, and a Kappa distribution of an energized population, peaking at approximately 20 keV. In this sense, we derived correlations between the parameters describing this high-energy population as a Kappa distribution function.

While no local time dependance was found, there is a correlation of the Kappa distribution parameters and the magnetospheric environment and also between the different parameters of the distribution. More than half of the periods analyzed have values of C, kT, and κ within specific ranges. Apart from this, there is a strong power law correlation between κ and C and between kT and C.

Acknowledgments
This work was carried out in the frame of the International Max Planck Research School (IMPRS) for Solar System Science at the Max Planck Institute for Solar System Research (MPS) as well as at the Mullard Space Science Laboratory (UCL) and the University of Michigan (UM). The German contribution of MIMI/LEMMS was in part financed by BMBF through DLR under contract 50OH1101 and by the Max Planck Gesellschaft. L. H. Regoli has received funds from an Impact Scholarship awarded by a collaboration between the University College London (UCL) and the Max Planck Society (MPG) and by a NASA Living With a Star grant (NNX16AL12G). A. J. C., G. H. J., and I. J. R. acknowledge support from the STFC consolidated grants to UCL-MSSL ST/K000977/1 and ST/N000722/1. Cassini data are available through NASA's planetary data system (PDS).

References

Achilleos, N., Arridge, C. S., Bertucci, C., Jackman, C. M., Dougherty, M. K., Khurana, K. K., & Russell, C. T. (2008). Large-scale dynamics of Saturn's magnetopause: Observations by Cassini. *Journal of Geophysical Research*, *113*, A11209. https://doi.org/10.1029/2008JA013265

Arridge, C. S., André, N., Bertucci, C. L., Garnier, P., Jackman, C. M., Németh, Z., et al. (2011). Upstream of Saturn and Titan. *Space Science Reviews*, *162*, 25–83.

Arridge, C. S., Khurana, K. K., Russell, C. T., Southwood, D. J., Achilleos, N., et al. (2008). Warping of Saturn's magnetospheric and magnetotail current sheets. *Journal of Geophysical Research*, *113*, A08217. https://doi.org/10.1029/2007JA012963

Backes, H., Neubauer, F. M., Dougherty, M. K., Achilleos, N., André, N., Arridge, C. S., et al. (2005). Titan's magnetic field signature during the first Cassini encounter. *Science*, *308*(5724), 992–995.

Bertucci, C., Achilleos, N., Dougherty, M. K., Modolo, R., Coates, A. J., Szego, K., et al. (2008). The magnetic memory of Titan's ionized atmosphere. *Science*, *321*(5895), 1475–1478.

Bertucci, C., Hamilton, D. C., Kurth, W. S., Hospodarsky, G., Mitchell, D., Sergis, N., et al. (2015). Titan's interaction with the supersonic solar wind. *Geophysical Research Letters*, *42*, 193–200. https://doi.org/10.1002/2014GL062106

Brain, D. A., Hurley, D., & Combi, M. R. (2010). The solar wind interaction with Mars: Recent progress and future directions. *Icarus*, *206*(1), 1–4. https://doi.org/10.1016/j.icarus.2009.10.020

Brandt, P. C., Dialynas, K., Dandouras, I., Mitchell, D. G., Garnier, P., & Krimigis, S. M. (2012). The distribution of Titan's high-altitude (out to ~50,000 km) exosphere from energetic neutral atom (ENA) measurements by Cassini/INCA. *Planetary and Space Science*, *60*(1), 107–114. https://doi.org/10.1016/j.pss.2011.04.014

Brecht, S. H., & Ledvina, S. A. (2006). The solar wind interaction with the Martian ionosphere/atmosphere. *Space Science Reviews*, *126*, 15–38. https://doi.org/10.1007/s11214-006-9084-z

Cravens, T. E., Robertson, I. P., Clark, J., Wahlund, J.-E., Waite, J. H. Jr., Ledvina, S. A., et al. (2005). Titan's ionosphere: Model comparisons with Cassini Ta data. *Geophysical Research Letters*, *32*, L12108. https://doi.org/10.1029/2005GL023249

Cravens, T. E., Robertson, I. P., Ledvina, S. A., Mitchell, D., Krimigis, S. M., & Waite, J. H. (2008). Energetic ion precipitation at Titan. *Geophysical Research Letters*, *35*, L03103. https://doi.org/10.1029/2007GL032451

Dialynas, K., Brandt, P. C., Krimigis, S. M., Mitchell, D. G., Hamilton, D. C., Krupp, N., & Rymer, A. M. (2013). The extended Saturnian neutral cloud as revealed by global ENA simulations using Cassini/MIMI measurements. *Journal of Geophysical Research: Space Physics*, *118*, 3027–3041. https://doi.org/10.1002/jgra.50295

Dialynas, K., Krimigis, S. M., Mitchell, D. G., Hamilton, D. C., Krupp, N., & Brandt, P. C. (2009). Energetic ion spectral characteristics in the Saturnian magnetosphere using Cassini/MIMI measurements. *Journal of Geophysical Research*, *114*, A01212. https://doi.org/10.1029/2008JA013761

Dialynas, K., Paranicas, C. P., Carbary, J. F., Kane, M., Krimigis, S. M., & Mauk, B. H. (2017). The Kappa-shaped particle spectra in planetary magnetospheres. In *Kappa Distributions* (pp. 481–522). Elsevier.

Edberg, N. J. T., Andrews, D. J., Bertucci, C., Gurnett, D. A., Holmberg, M. K. G., Jackman, C. M., et al. (2015). Effects of Saturn's magnetospheric dynamics on Titan's ionosphere. *Journal of Geophysical Research: Space Physics*, *120*, 8884–8898. https://doi.org/10.1002/2015JA021373

Edberg, N. J. T., Andrews, D. J., Shebanits, O., Ågren, K., Wahlund, J.-E., Opgenoorth, H. J., et al. (2013). Extreme densities in Titan's ionosphere during the T85 magnetosheath encounter. *Geophysical Research Letters*, *40*, 2879–2883. https://doi.org/10.1002/grl.50579

Garnier, P., Dandouras, I., Toublanc, D., Roelof, E. C., Brandt, P. C., Mitchell, D. G., et al. (2010). Statistical analysis of the energetic ion and ENA data for the Titan environment. *Planetary and Space Science*, *58*, 1811–1822.

Gronoff, G., Lilensten, J., & Modolo, R. (2009). Ionization processes in the atmosphere of Titan II. Electron precipitation along magnetic field lines. *Astronomy & Astrophysics*, *506*, 965–970. https://doi.org/10.1051/0004-6361-200912125

Hartle, R. E., Sittler, E. C., Neubauer, F. M., Johnson, R. E., Smith, H. T., Crary, F., et al. (2006). Preliminary interpretation of Titan plasma interaction as observed by the Cassini plasma spectrometer: Comparisons with Voyager 1. *Geophysical Research Letters*, *33*, L08201. https://doi.org/10.1029/2005GL024817

Kabanovic, S., Simon, S., Neubauer, F. M., & Meeks, Z. (2017). An empirical model of Titan's magnetic environment during the Cassini era: Evidence for seasonal variability. *Journal of Geophysical Research: Space Physics*, *122*, 11,076–11,085. https://doi.org/10.1002/2017JA024402

Krimigis, S. M., Mitchell, D. G., Hamilton, D. C., Livi, S., Dandouras, J., Jaskulek, S., et al. (2004). Magnetosphere imaging instrument (MIMI) on the Cassini mission to Saturn/Titan. *Space Science Reviews*, *114*, 233–329. https://doi.org/10.1007/s11214-004-1410-8

Krimigis, S. M., Sergis, N., Mitchell, D. G., Hamilton, D. C., & Krupp, N. (2007). A dynamic, rotating ring current around Saturn. *Nature*, *450*, 1050–1053. https://doi.org/10.1038/nature06425

Krupp, N., Roussos, E., Kollmann, P., Paranicas, C., Mitchell, D. G., Krimigis, S. M., et al. (2012). The Cassini Enceladus encounters 2005–2010 in the view of energetic electron measurements. *Icarus*, *218*(1), 433–447. https://doi.org/10.1016/j.icarus.2011.12.018

Krupp, N., Roussos, E., Lagg, A., Woch, J., Müller, A. L., Krimigis, S. M., et al. (2009). Energetic particles in Saturn's magnetosphere during the Cassini nominal mission (July 2004–July 2008). *Planetary and Space Science*, *57*(14–15), 1754–1768. https://doi.org/10.1016/j.pss.2009.06.010

Livadiotis, G. (2015). Introduction to special section on Origins and Properties of Kappa Distributions: Statistical background and properties of kappa distributions in space plasmas. *Journal of Geophysical Research: Space Physics*, *120*, 1607–1619. https://doi.org/10.1002/2014JA020825

Livadiotis, G. (2017). Chapter 1 — Statistical background of kappa distributions: Connection with nonextensive statistical mechanics. In G. Livadiotis (Ed.), *Kappa Distributions* (pp. 3–63). Elsevier. https://doi.org/10.1016/B978-0-12-804638-8.00001-2

Livadiotis, G., & McComas, D. J. (2013). Understanding kappa distributions: A toolbox for space science and astrophysics. *Space Science Reviews*, *175*(1), 183–214.

Mauk, B. H., Mitchell, D. G., McEntire, R. W., Paranicas, C. P., Roelof, E. C., Williams, D. J., et al. (2004). Energetic ion characteristics and neutral gas interactions in Jupiter's magnetosphere. *Journal of Geophysical Research*, *109*, A09S12. https://doi.org/10.1029/2003JA010270

Németh, Z., Szego, K., Bebesi, Z., Erdős, G., Foldy, L., Rymer, A., et al. (2011). Ion distributions of different Kronian plasma regions. *Journal of Geophysical Research*, *116*, A09212. https://doi.org/10.1029/2011JA016585

Neubauer, F. M., Gurnett, D. A., Scudder, J. D., & Hartle, R. E. (1984). Titan's magnetospheric interaction. In T. Gehrels & M. S. Matthews (Eds.), *Saturn*. Tucson, AZ: University of Arizona Press.

Regoli, L. H., Roussos, E., Feyerabend, M., Jones, G. H., Krupp, N., Coates, A. J., et al. (2016). Access of energetic particles to Titan's exobase: A study of Cassini's T9 flyby. *Planetary and Space Science*, *130*, 40–53. https://doi.org/10.1016/j.pss.2015.11.013

Roussos, E., Jackman, C. M., Thomsen, M. F., Kurth, W. S., Badman, S. V., Paranicas, C., et al. (2017). Solar energetic particles (SEP) and galactic cosmic rays (GCR) as tracers of solar wind conditions near Saturn: Event lists and applications. *Icarus*, *300*, 47–71. https://doi.org/10.1016/j.icarus.2017.08.040

Russell, C. T., Luhmann, J. G., & Strangeway, R. J. (2006). The solar wind interaction with Venus through the eyes of the Pioneer Venus Orbiter. *Planetary and Space Science*, *54*, 1482–1495. https://doi.org/10.1016/j.pss.2006.04.025

Rymer, A. M., Smith, H. T., Wellbrock, A., Coates, A. J., & Young, D. T. (2009). Discrete classification and electron energy spectra of Titan's varied magnetospheric environment. *Geophysical Research Letters*, *36*, L15109. https://doi.org/10.1029/2009GL039427

Sergis, N., Krimigis, S. M., Mitchell, D. G., Hamilton, D. C., Krupp, N., Mauk, B. M., et al. (2007). Ring current at Saturn: Energetic particle pressure in Saturn's equatorial magnetosphere measured with Cassini/MIMI. *Geophysical Research Letters*, *34*, L09102. https://doi.org/10.1029/2006GL029223

Sergis, N., Krimigis, S. M., Mitchell, D. G., Hamilton, D. C., Krupp, N., Mauk, B. H., et al. (2009). Energetic particle pressure in Saturn's magnetosphere measured with the magnetospheric imaging instrument on Cassini. *Journal of Geophysical Research*, *114*, A02214. https://doi.org/10.1029/2008JA013774

Simon, S., van Treeck, S. C., Wennmacher, A., Saur, J., Neubauer, F. M., Bertucci, C. L., & Dougherty, M. K. (2013). Structure of Titan's induced magnetosphere under varying background magnetic field conditions: Survey of Cassini magnetometer data from flybys TA-T85. *Journal of Geophysical Research: Space Physics*, *118*, 1679–1699. https://doi.org/10.1002/jgra.50096

Simon, S., Wennmacher, A., Neubauer, F. M., Bertucci, C. L., Kriegel, H., Saur, J., et al. (2010). Titan's highly dynamic magnetic environment: A systematic survey of Cassini magnetometer observations from flybys TA–T62. *Planetary and Space Science*, *58*(10), 1230–1251. https://doi.org/10.1016/j.pss.2010.04.021

Slavin, J. A., Elphic, R. C., Russell, C. T., Scarf, F. L., Wolfe, J. H., Mihalov, J. D., et al. (1980). The solar wind interaction with Venus: Pioneer Venus observations of bow shock location and structure. *Journal of Geophysical Research*, *85*, 7625–7641. https://doi.org/10.1029/JA085iA13p07625

Smith, H. T., Mitchell, D. G., Johnson, R. E., & Paranicas, C. P. (2009). Investigation of energetic proton penetration in Titan's atmosphere using the Cassini INCA instrument. *Planetary and Space Science*, *57*(13), 1538–1546. https://doi.org/10.1016/j.pss.2009.03.013

Smith, H. T., & Rymer, A. M. (2014). An empirical model for the plasma environment along Titan's orbit based on Cassini plasma observations. *Journal of Geophysical Research: Space Physics*, *119*, 5674–5684. https://doi.org/10.1002/2014JA019872

Thomsen, M. F., Coates, A. J., Jackman, C. M., Sergis, N., Jia, X., & Hansen, K. C. (2018). Survey of magnetosheath plasma properties at Saturn and inference of upstream flow conditions. *Journal of Geophysical Research: Space Physics*, *123*, 2034–2053. https://doi.org/10.1002/2018JA025214

Thomsen, M. F., Reisenfeld, D. B., Delapp, D. M., Tokar, R. L., Young, D. T., Crary, F. J., et al. (2010). Survey of ion plasma parameters in Saturn's magnetosphere. *Journal of Geophysical Research*, *115*, A10220. https://doi.org/10.1029/2010JA015267

Vasyliunas, V. M. (1968). A survey of low-energy electrons in the evening sector of the magnetosphere with OGO 1 and OGO 3. *Journal of Geophysical Research*, *73*, 2839–2884. https://doi.org/10.1029/JA073i009p02839

Wei, H. Y., Russell, C. T., Dougherty, M. K., Neubauer, F. M., & Ma, Y. J. (2010). Upper limits on Titan's magnetic moment and implications for its interior. *Journal of Geophysical Research*, *115*, E10007. https://doi.org/10.1029/2009JE003538

Young, D. T., Berthelier, J.-J., Blanc, M., Burch, J. L., Bolton, S., Coates, A. J., et al. (2005). Composition and dynamics of plasma in Saturn's magnetosphere. *Science*, *307*, 1262–1266. https://doi.org/10.1126/science.1106151

Young, D. T., Berthelier, J. J., Blanc, M., Burch, J. L., Coates, A. J., Goldstein, R., et al. (2004). Cassini plasma spectrometer investigation. *Space Science Reviews*, *114*, 1–112.